Environmental Science & Technology Letters

Letter

Cite This: Environ. Sci. Technol. Lett. 2018, 5, 668−674

pubs.acs.org/journal/estlcu

Multifold Enhancement of Loose Nanofiltration Membrane Performance by Intercalation of Surfactant Assemblies

Linglong Shan,[†,‡] Yuanzhe Liang,[§] Liudmyla Prozorovska,[§] G. Kane Jennings,[∥] Shulan Ji,[†] and Shihong Lin*[,‡,∥]

[†]Beijing Key Laboratory for Green Catalysis and Separation, College of Environmental and Energy Engineering, Beijing University of Technology, Beijing 100124, P. R. China

[‡]Department of Civil and Environmental Engineering, Vanderbilt University, Nashville, Tennessee 37235, United States

[§]Interdisciplinary Material Science Program, Vanderbilt University, Nashville, Tennessee 37235, United States

[∥]Department of Chemical and Biomolecular Engineering, Vanderbilt University, Nashville, Tennessee 37235, United States

Supporting Information

ABSTRACT: Enhancing the membrane water permeability without undermining selectivity has strong potential to reduce the cost of loose nanofiltration (LNF) which attracts growing interest in water and wastewater treatments. Herein, we report a novel polyelectrolyte multilayer LNF membrane with intercalated surfactant self-assemblies. The LNF membranes with integrated surfactant self-assemblies exhibit outstanding permeability to water and selectivity to organic macromolecules such as humic acid and methyl blue. Specifically, the integration of surfactant self-assemblies, SSA, enhances the water permeability by more than 5-fold compared to the reference LNF membrane and, at the same time, increases humic acid rejection from 93% to 98%. The SSA integrated LNF membranes also demonstrate superior performance in terms of permselectivity compared to other membranes in the literature for similar separation (humic acid removal).

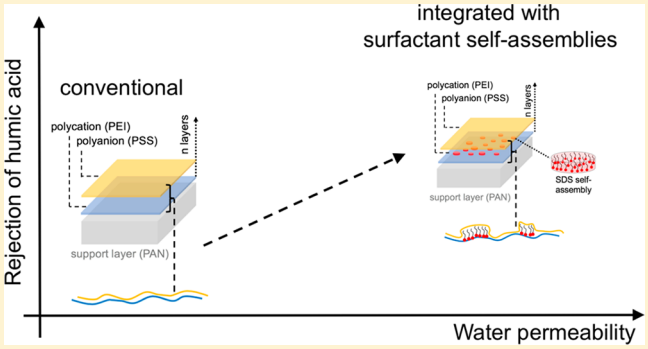

INTRODUCTION

Loose nanofiltration (LNF) membrane is a class of membranes with a pore size at the boundary between nanofiltration (NF) and ultrafiltration (UF). Unlike tight NF membranes, which are usually employed for brackish water desalination[1] and water softening,[2] LNF is effective in removing organic macromolecules but not salts.[3−5] In return, the water permeability of a typical LNF membrane is significantly higher than that of a tight NF membrane, allowing much faster filtration at lower pressure. On the other hand, LNF membranes can remove relatively small organic macromolecules that UF membranes fail to reject to a satisfactory extent. For these reasons, LNF has been actively explored for applications in removing natural organic matter (NOM),[6] pharmaceuticals,[7] hormones,[8] pesticides,[9] and desalting dye wastewater.[10] Notably, by removing NOM from feedwater, LNF can significantly reduce the formation of disinfection byproduct of which NOM is the precursor.[11−13]

The most important membrane performance metrics are rejection of target solutes and water permeability, with the former determining whether the membrane can be used for target applications, and the later affecting the required hydraulic pressure or membrane area, which in turn influence the overall cost of the treatment. A recent analysis suggests that increasing water permeability of reverse osmosis (RO) membranes beyond the state-of-the-art has only marginal contribution to reducing the energy consumption or membrane area, mostly due to concentration polarization (CP).[14] However, for LNF applications, CP has a much smaller impact on energy consumption or flux because (1) LNF membranes are permeable to solutes that contribute to a large fraction of the feed osmotic pressure and thus do not cause significant accumulation of salts near the membrane surface, and (2) the feed osmotic pressure is very small for most LNF applications. Therefore, enhancing the water permeability of an LNF membrane without sacrificing its rejection of target solutes will have significant positive impact on reducing either the capital or operating cost of LNF.[15] Specifically, for the same operating pressure, an LNF membrane with enhanced permeability will significantly improve the water flux and thus reduce the required membrane area for achieving a target productivity, thereby reducing the capital cost. For the same membrane area, the use of an LNF membrane with enhanced water permeability will significantly reduce the operating pressure

Received: August 16, 2018
Revised: September 27, 2018
Accepted: September 28, 2018
Published: September 28, 2018

DOI: 10.1021/acs.estlett.8b00430
Environ. Sci. Technol. Lett. 2018, 5, 668−674

required to achieve a certain flux, thereby reducing the energy cost.

In recent years, layer-by-layer (LbL) deposition of polyelectrolytes has been actively investigated as a method to fabricate NF membranes with polyelectrolyte multilayers as the active layer.[16−24] This approach has the general advantages of high flexibility in tuning active layer chemistry,[25,26] high water permeability,[27] low fouling propensity,[28,29] chlorine resistance,[30] and absence of any toxic organic solvent in manufacturing.

Herein, we report a novel and simple approach for drastically enhancing the performance of LNF membranes fabricated using LbL deposition of polyelectrolyte. The key innovation in this new approach is the integration of anionic surfactants into the polyelectrolyte active layer. In this study, we fabricate LNF membranes made of polyethylenimine (PEI) and polystyrenesulfonate (PSS) with and without the integration of sodium dodecyl sulfate (SDS) into the PEI/PSS active layer. We characterize the material properties and test the performance of the LNF membrane with SDS integration and compare that to a reference LNF membrane without SDS integration. Finally, we also evaluate the stability of the SDS-integrated LNF membrane in long-term operation.

MATERIALS AND METHODS

Chemical and Materials. Polyacrylonitrile (PAN) UF membranes (MWCO = 50 kDa) were purchased from GE Healthcare Life Sciences. Humic acid (HA), PEI (Mw = 750 000), PSS (Mw = 10 000 000), sodium dodecyl sulfate (SDS, ≥99%), hydrochloric acid (HCl, 32 wt % in H_2O), potassium chloride (KCl, ≥99%), glutaraldehyde (50 wt % in H_2O), methyl blue (MB, Mw = 799.8), Na_2SO_4 (≥99%), $MgSO_4$ (≥99.5%), $MgCl_2$ (≥99.99%), NaCl (≥99%), $CaCl_2$ (≥97%), and sodium hydroxide (NaOH, ≥98%) were purchased from Sigma-Aldrich. All these solutes were of reagent grade and used without any purification.

Fabrication of Reference and SDS-Integrated LNF Membrane. The reference LNF membrane was fabricated via LbL deposition of PEI and PSS (chemical structure shown in Figure 1A) onto a commercial PAN ultrafiltration membrane

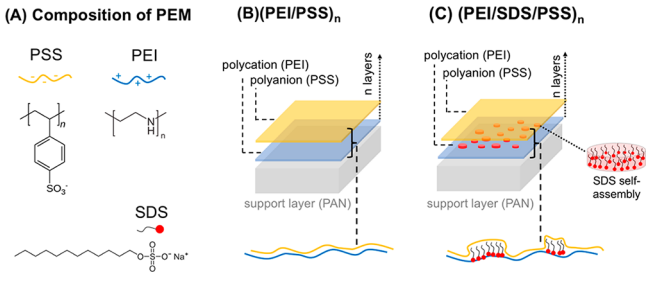

Figure 1. (A) Chemical structure of the three major chemical components used to construct the polyelectrolyte multilayer. (B) Schematic of a PEI/PSS polyelectrolyte multilayer on a PAN substrate. (C) Schematic of a PEI/SDS/PSS polyelectrolyte multilayer on a PAN substrate.

as the support layer (Figure 1B). The PAN UF membrane was first hydrolyzed using 2.0 M NaOH to acquire negative charge for depositing the first positively charged PEI layer. The hydrolyzed PAN substrate was immersed in an aqueous solution of 1.0 g/L PEI polycation for 30 min, rinsed with water, and then immersed in an aqueous solution of 2.0 g/L of PSS polyanion for another 30 min. The resulting membrane has one composite layer of PEI/PSS bound by electrostatic interaction and is referred to as the PAN-$(PEI/PSS)_1$ membrane, with the subscript "1" representing one PEI/PSS layer. A similar procedure was repeated to deposit two additional PEI/PSS layers. The resulting PAN-$(PEI/PSS)_3$ membrane with three PEI/PSS layers was used as the baseline for performance comparison. Cross-linking with glutaraldehyde (0.2 g/L at 40 °C for 24 h) was performed on some membrane samples. The samples were not cross-linked unless specified in the discussion or caption.

The integration of SDS into the polyelectrolyte multilayer to form the PAN-$(PEI/SDS/PSS)_3$ membrane followed the same procedure as preparing the PAN-$(PEI/PSS)_3$ reference membrane, except that extra SDS deposition steps were introduced before PSS deposition (Figure 1C). Specifically, after each step of PEI deposition, the membrane with PEI on the surface was immersed into an aqueous solution of SDS of a certain concentration (from 0 to 6.5 g/L) for 30 min. The SDS coated PEI surface was then further subject to PSS deposition as in preparing the PAN-$(PEI/PSS)_3$ reference membrane. We postulate that SDS self-assembled on the PEI surface as either monolayers or bilayers that lead to the lowest system free energy due to the interlayer and/or lateral hydrophobic interaction (Figure 1C).[31−33] It is challenging to directly prove this postulate by observing the morphology of a PEI surface coated with SDS, because the intrinsic roughness of a PEI layer is significantly larger than the thickness of an SDS monolayer or bilayer. However, self-assemblies of surfactants on a solid−water interface have been extensively observed in previous studies.[34−38] In this study, we will indirectly prove the above postulate by measuring the surface morphology of a smooth silicon wafer with adsorbed SDS using atomic force microscopy (AFM).

In addition to using the approach the sequential deposition of polyelectrolytes and SDS, we also prepared LNF membranes using two other approaches for SDS integration. In the first approach, SDS was employed to replace the PSS polyanions and the PSS deposition steps were eliminated. In the second approach, PSS and SDS were co-deposited onto the PEI surface simultaneously as a mixture instead of sequentially as separate reagents. In each approach, the polyelectrolyte multilayer was composed of three composite layers. LNF membranes obtained using these two approaches were compared with the reference PAN-$(PEI/PSS)_3$ membrane and the PAN-$(PEI/SDS/PSS)_3$ membrane for performance.

Membrane Characterization and Performance Evaluation. Zeta potentials of the membrane surface at different stages of fabrication were measured using a streaming potential technique (SurPASS electrokinetic analyzer, Anton Paar, Austria) with 0.1 mM KCl as the electrolyte solution. Scanning electron microscopy (SEM, Zeiss Merlin) was performed to evaluate the surface morphology of the membranes. AFM was also conducted to assess the surface morphology and quantify the surface roughness. The surface wetting property of the membranes was quantified by measuring the water contact angle using an optical goniometer. To acquire molecular level information on the active layers fabricated using different methods, we also performed polarization modulation-infrared reflection absorption spectroscopy (PM-IRRAS) on different polyelectrolyte multilayers deposited on Au/Si substrates using a Bruker Tensor 27 Fourier transform infrared spectroscopy. The detailed procedure of preparing such samples is reported in the Supporting Information.

The NF performance of the membranes was evaluated using a cross-flow filtration cell with an active area of 15.9 cm^2 and a

DOI: 10.1021/acs.estlett.8b00430
Environ. Sci. Technol. Lett. 2018, 5, 668−674

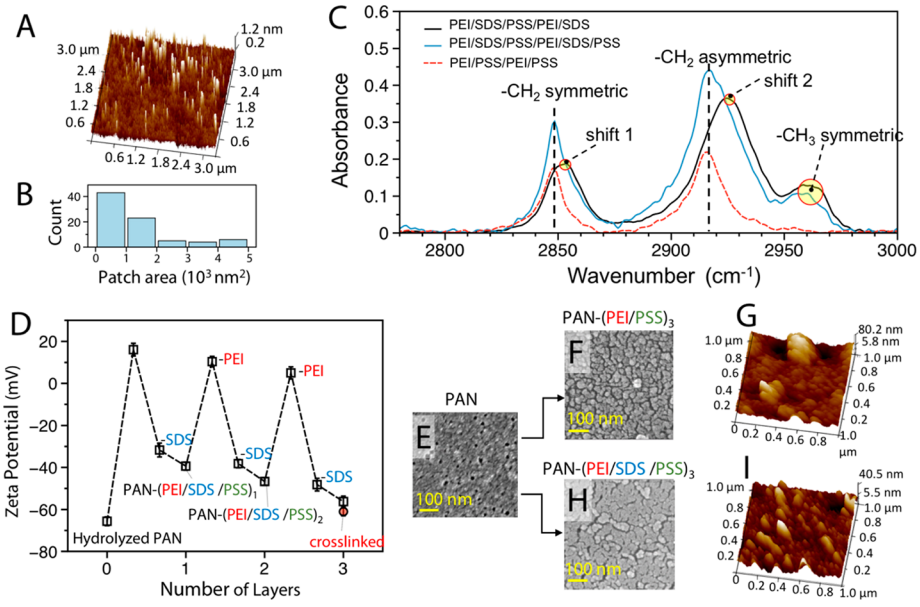

Figure 2. (A) Morphology of self-assembled SDS patches on an originally smooth and positively charged silicon wafer surface. (B) Size distribution of self-assembled SDS patches obtained from analyzing AFM images using ImageJ. (C) FTIR spectra of PEI/SDS/PSS/PEI/SDS (black), PEI/SDS/PSS/PEI/SDS/PSS (blue), and PEI/PSS/PEI/PSS (red) films. (D) Zeta potentials of the membrane surfaces at different stages of fabricating the PAN-$(PEI/SDS/PSS)_3$ membrane as obtained by streaming potential measurements. "-PEI" and "-SDS" represent membranes with its top surfaces being PEI and SDS, respectively. (E) SEM image of hydrolyzed PAN membrane. (H and I) SEM and AFM images of the PAN-$(PEI/SDS/PSS)_3$ membrane, respectively. (F and G) SEM and AFM images of the reference PAN-$(PEI/PSS)_3$ membrane, respectively. The Sq of the PAN-$(PEI/SDS/PSS)_3$ and PAN-$(PEI/PSS)_3$ membranes based on AFM images are 8.46 and 17.5 nm, respectively.

cross-flow velocity of 2.9 cm s^{-1}. Two major performance metrics were evaluated, including water flux and solute rejection. Because the primary function of the LNF membrane fabricated in this study is to remove HA as a model NOM in feedwater, HA rejection was assessed systematically using 10 mg/L HA as the feed solution with and without 1 mM $CaCl_2$. However, rejection of other solutes, including methyl blue and a series of monovalent and divalent salts, was also assessed for the PAN-$(PEI/SDS/PSS)_3$ membrane. The concentrations for methyl blue and ionic salts were 0.5 g/L and 0.1 g/L, respectively. In all experiments, the applied pressure was 60 psi (or 4.1 bar).

RESULTS AND DISCUSSION

Morphology and Surface Property of Polyelectrolyte Multilayer. As revealed by AFM images (Figure 2A as an example), a smooth silicon wafer surface with adsorbed SDS has a high density of patches with a thickness of 1.38 ± 0.25 nm which is close to the thickness of a surface-bound SDS monolayer measured using X-ray reflectivity.[39] The size distribution of these patches (Figure 2B) suggests that they are of a general geometry of "pancakes" instead of "globes" that would have been expected for adsorbed micelles (we note that the vertical axis and horizontal axes in Figure 2A are of very different scales). Similar formation of "pancake-like" self-assemblies is expected on a membrane with a PEI top layer, even though it cannot be confirmed using AFM due to the large intrinsic roughness of a PEI surface.

FTIR spectra of dual-layer PEI/PSS (red) and PEI/SDS/PSS (blue) films show similar peaks for symmetric and asymmetric CH_2 stretching (Figure 2C).[40] However, the presence of SDS increased the bandwidth of both peaks, which is consistent with reduced crystallinity (increased number of gauche CH_2) of the PEI/SDS/PSS films.[41] The reduced crystallinity enhances the free volume of the polyelectrolyte multilayer and increases the water permeability. The presence of SDS can also be verified by the peak corresponding to symmetric CH_3 stretching (Figure 2C) which is absent in the PEI/PSS film. When SDS was the top layer (black curve in Figure 2C), peaks for both asymmetric and symmetric CH_2 stretching experienced a red shift that is characteristic of self-assembled structures similar to micelles.[42,43]

The zeta potentials of the membrane sample at different steps of the LbL deposition suggest the successful deposition of each species onto the membrane surface (Figure 2D). Specifically, the hydrophilized PAN surface was highly negatively charged (−65.6 mV) due to the presence of abundant hydroxyl groups, as confirmed by ATR-FTIR spectroscopy (Figure S1). The deposition of PEI onto the hydrolyzed PAN surface significantly increased the surface potential to the extent that the PAN−PEI surface became positively charged. The deposition of SDS onto the PAN−PEI surface reversed the surface charge, rendering the PAN−PEI/SDS surface negatively charged.

If the LbL depositon is driven by electrostatic attraction and the surface charge was assumed to smear out homogeneously, then subsequent depositon of highly negatively charged PSS to a overall moderately negatively charged PAN−PEI/SDS surface should have been unlikely. However, the measured zeta potential suggests the occurrence of such deposition, as the zeta potential was further and consistently reduced by ∼10 mV after each PSS-depositon step. The successful deposition of PSS onto the negatively charged PAN−PEI/SDS surface may be explained by the surface charge heterogeneity of the PAN−PEI/SDS surface. Once the PAN−PEI/SDS was immersed into a PSS solution, the sulfonate moieties on the PSS partially adsorbed onto the amine groups on the PEI that had not been occupied by the SDS molecules and thus further reduced the surface zeta potenital. Cross-linking the PEI with

DOI: 10.1021/acs.estlett.8b00430
Environ. Sci. Technol. Lett. 2018, 5, 668−674

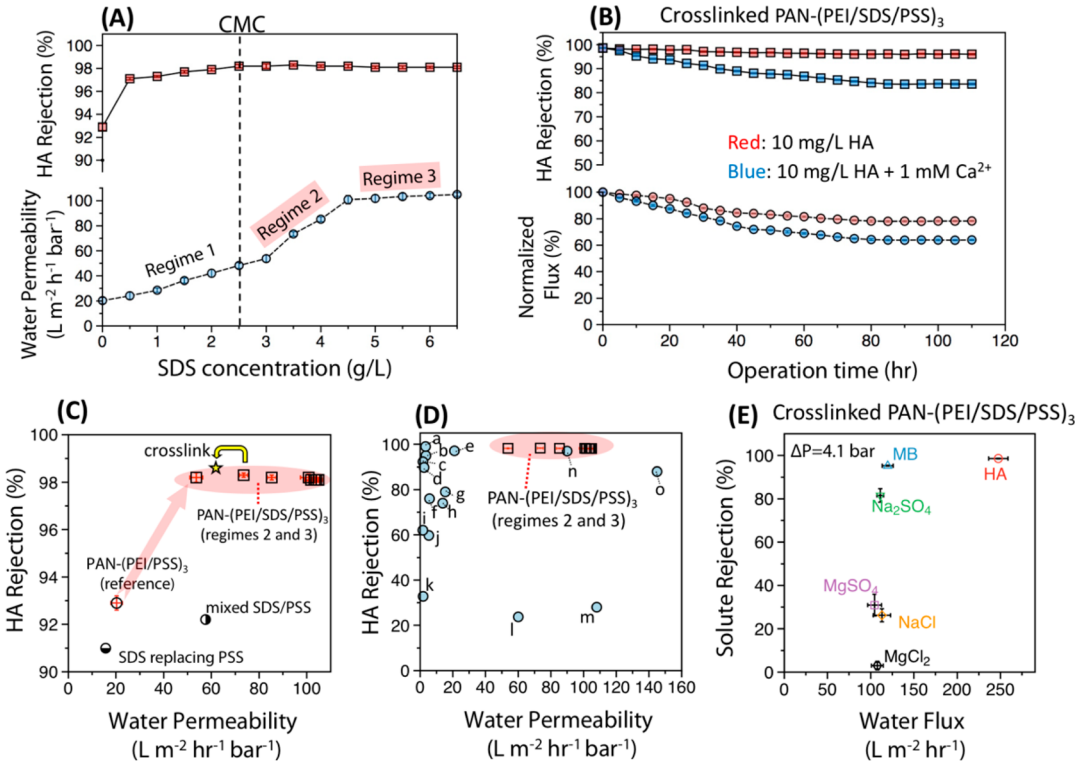

Figure 3. (A) Water permeability (bottom) and HA rejection (top) of the PAN-$(PEI/SDS/PSS)_3$ LNF membrane with different SDS concentration in the solutions for SDS deposition. (B) Normalized flux (bottom) and HA rejection (top) of a cross-linked PAN-$(PEI/SDS/PSS)_3$ LNF membrane over 100 h of filtration experiments with 10 mg/L HA with (blue) and without (red) Ca^{2+} (1 mM). (C) HA rejection and water permeability of the PAN-$(PEI/SDS/PSS)_3$ membranes, the reference PAN-$(PEI/PSS)_3$ membrane, and SDS-integrated membranes fabricating using two alternative approaches as indicated in the figure. The data from regimes 2 and 3 (see Figure 3A) are highlighted in red. The star represents the performance of the selected cross-linked sample (with 3.5 g L^{-1} SDS). (D) HA rejection and water permeability of the PAN-$(PEI/SDS/PSS)_3$ membranes as compared to other NF membranes reported in literature. The detailed performance for each data point is reported in the Supporting Information (Table S1). (E) Water fluxes and rejections of different solutes measured using cross-linked PAN-$(PEI/SDS/PSS)_3$ membranes.

glutaraldehyde (0.2 g/L at 40 °C for 24 h) at the end of fabricating the PAN-$(PEI/SDS/PSS)_3$ membrane did not seem to affect the zeta potential to any significant extent (Figure 2D).

Comparing the SEM images of the surface of the PAN-$(PEI/SDS/PSS)_3$ membrane (Figure 2H) and PAN-$(PEI/PSS)_3$ membrane (Figure 2F) suggests that the presence of SDS resulted in a smoother surface, which is also confirmed by the surface roughness analysis based on AFM images (Figure 2I, 2G). The surface of the PAN-$(PEI/PSS)_3$ membrane is more "granular", which is typical of polyelectrolyte multilayer membranes developed by LbL deposition.

Performance of the PAN$(PEI/SDS/PSS)_3$ LNF Membrane. The water permeability and HA rejection of PAN-$(PEI/SDS/PSS)_3$ LNF membranes depend on the SDS concentration used in the SDS deposition step (Figure 3A). The baseline PAN-$(PEI/PSS)_3$ membrane without any SDS integration achieved an HA rejection of ~93% (in the absence of Ca^{2+}). The presence of SDS, even at a low concentration of 0.5 g/L, enhanced the HA rejection to 97%. Further increasing the SDS concentration beyond its critical micelle concentration (CMC) leads to a stable HA rejection higher than 98%. In a previous study using the same compositions of PEI and PSS without SDS integration, enhanced HA rejection was achieved by increasing the PSS concentration or the number of PEI/PSS layers. However, even with 5 g/L (as compared to 2 g/L used in this study) and 6 layers (as compared to 3 layers in this study) of PEI/PSS, the HA rejection in that previous study never reached 98%.[44]

The even more salient effect of SDS integration was on enhancing the water permeability of the LNF membranes. Steady and significant enhancement of water permeability was observed with increasing concentration of the SDS solution used in LbL deposition (Figure 3A). Increasing the SDS concentration from zero to CMC more than doubled the water permeability (regime 1). Further increasing the SDS concentration to 4.5 g/L enhanced the water permeability by 5-fold (regime 2). Beyond 4.5 g/L, further increasing SDS concentration did not seem to have any observable impact on water permeability (regime 3). The maximum water permeability was beyond 100 L m^{-2} h^{-1} bar^{-1}, which is a several fold increase compared to that of the reference PAN-$(PEI/PSS)_3$ membrane.

There is a clear difference between regime 1 (below CMC) and regime 2 (above CMC) in the effectiveness of increasing SDS concentration on enhancing water permeability. Below CMC, increasing SDS concentration from 0 to 2.5 g/L enhanced the water permeability from 20.3 to 48.2 L m^{-2} h^{-1} bar^{-1} (slope = 11.1). Beyond CMC, increasing the SDS concentration from 2.5 to 4.5 g/L enhanced the water permeability from 48.2 to 100.8 L m^{-2} h^{-1} bar^{-1} (slope = 26.3). The "effectiveness" of SDS addition in enhancing water permeability, defined as permeability enhancement per increment of SDS concentration, is ~2.4 times higher in regime 2 than in regime 1.

DOI: 10.1021/acs.estlett.8b00430
Environ. Sci. Technol. Lett. 2018, 5, 668−674

Suprisingly, the rejection of HA was also enhanced by the integration of SDS. It was possible that rejection of HA by the LNF membrane is attributable not only to size and Donnan exclusions but also to absorptive interaction with the active layer. Because HA has a signifcant fraction of hydrophobic moieties, the enhanced hydrophobicity of the $(PEI/SDS/PSS)_3$ active layer, which is caused by the abundant alky groups from SDS and confirmed by the measured water contact angle (Figure S2), contributed to the enhanced rejection of HA.[45,46]

When the SDS concentration is below CMC, SDS exists in solution as single molecules. In this scenario, SDS molecules can adsorb onto the PEI surface via electrostatic attraction and exists as sparsely adsorbed single molecules. The formation of self-assembled patches (monolayer or bilayer) is possible but less likely than in regime 2. When the SDS concentration is beyond CMC, SDS exists as micelles in the solution and adsorbs onto the PEI surface as spherical self-assemblies. The deformation of micelles to bilayers increases the extent of both electrostatic attraction between sulfonate groups and the PEI surface and the hydrophobic attraction between the alkyl chains, which is energetically favorable. The difference in the state of the surface bound SDS and in the effectiveness of water permeability enhancement between the two regimes suggests that local self-assembled SDS patches are likely responsible for the drastic permeability enhancement. This may be explained by the local disruption of the dense PEI/PSS active layer, which is similar to the mechanism of permeability enhancement by impregnating inorganic nanoparticles and is supported by the possible reduction in PEI/PSS crystallinity as evidenced by the corresponding IR spectra of the active layers (Figure 2C). The MWCOs (i.e., 90% rejection) of the $(PEI/PSS)_3$ and $(PEI/SDS/PSS)_3$ layers were measured to be 3K and 4K, respectively, using polyethylene glycol as the model solutes.

The stability of the cross-linked PAN-$(PEI/SDS/PSS)_3$ LNF membrane was evaluated by monitoring its water flux and HA rejection for over 100 h of operation (Figure 3B). The cross-linking step is typically required to enhance the long-term stability of the LNF membrane prepared via LbL deposition. Both water flux and HA rejection decreased slightly in the first 2 days of operation but eventually stabilized. Specifically, the water flux decreased by ~15% to 85% of the initial flux and the HA rejection dropped from 98.6% to 96% in the absence of Ca^{2+}. Crossflow flushing of the membrane surface with DI water recovered the flux to 89% of the initial flux, which indicates that fouling was partially irreversible. The flux decline was aggravated by the presence of Ca^{2+} due to the well-known bridging effect.[47] The compromised HA rejection in the presence of Ca^{2+} has not been clearly understood but has nontheless been reported in literature.[48,49] In both cases, the decline of HA rejection over time may be explained by the gradual depletion of hydrophobic adsorption sites, as hydrophobic interaction between HA and the alky chains of SDS possibly contributed to HA rejection as we discussed above.

We also note the PAN-$(PEI/SDS/PSS)_3$ is chemically relatively stable in LNF application. Prolonged filtration with the as-prepared PAN-$(PEI/SDS/PSS)_3$ using DI water only leached ~0.04% of total organic carbon to the permeate. However, swelling of the cross-linked active layer was observed when the ionic strength was increased to 100 mM (NaCl), as evidenced by slightly enhanced water permeability (25% increase) and reduced HA rejection (from 98.3% to 96.4%).

We also prepared LNF membranes using two other approaches with SDS integration, one with SDS replacing PSS and the other with simultaneous deposition of SDS and PSS, as described in the Materials and Method section. However, neither approach led to the significant performance enhancement achieved by the PAN-$(PEI/SDS/PSS)_3$ membranes with an SDS concentration higher than CMC (Figure 3C). Compared with the performance of other LNF membranes reported in literature, the PAN-$(PEI/SDS/PSS)_3$ LNF membranes achieved relatively good performance in both water permeability and HA rejection (Figure 3D).[44,50−58]

Lastly, the rejection and flux of LNF using the cross-linked PAN-$(PEI/SDS/PSS)_3$ membrane for removing different solutes were also evaluated, and the results are presented in Figure 3E. The rejections of organic macromolecules such as HA and methyl blue (MB) are both above 95%. The rejections of Na_2SO_4, $MgSO_4$, NaCl, and $MgCl_2$ are 81.6%, 30.9%, 26.2%, and 3.0%, respectively. Apparently, the Donnan effect played a dominant role in ion rejection by the PAN-$(PEI/SDS/PSS)_3$ membrane, evidenced by the higher rejection for Na^+ than Mg^{2+}, even though hydrated Mg^{2+} is larger than hydrated Na^+. Such a phenomenon has been observed with other membranes including commercial NF membranes.[59,60] The high rejection of organic macromolecules and relatively low rejection of ions render this membrane particularly suitable for applications where salt rejection is unnecessary, as in treating groundwater with low total dissolved solids, or where salt rejection is even undesirable, as in dye wastewater desaling where salt should pass through and dye should be retained.

IMPLICATIONS

For applications with LNF membranes that do not reject salts, enhancing the water permeability without sacrificing rejection of the target contaminants can significantly reduce the overall cost of the treatment processes, thereby rendering them more economically viable. Extensive effort has been invested to pursue this goal by exploring new membrane materials and integrating nanomaterials into existing membranes to form nanocomposite membranes. The approach we report herein represents a novel, highly promising, and practical method for enhancing LNF membrane performance using self-assemblies of commonly available and low-cost surfactants. While the exact mechanism of the drastic performance enhancement needs to be further elucidated, the reported approach opens a new door to vast opportunities, as many different types of surfactants, polyelectrolytes, and structures of polyelectrolyte multilayer can be investigated to optimize membrane performance for different applications.

ASSOCIATED CONTENT

Supporting Information

The Supporting Information is available free of charge on the ACS Publications website at DOI: 10.1021/acs.estlett.8b00430.

Details about the preparation of polyelectrolyte films on substrates for PM-IRRAS measurement; FTIR spectrum of the hydrolyzed PAN membrane; water contact angles of different membrane samples; Table S1 that contains the detailed information on the composition and performance of LNF membranes compared in Figure 3D (PDF)

DOI: 10.1021/acs.estlett.8b00430
Environ. Sci. Technol. Lett. 2018, 5, 668−674

AUTHOR INFORMATION

Corresponding Author

*E-mail: shihong.lin@vanderbilt.edu. Phone: +1(615)322-7226.

ORCID

G. Kane Jennings: 0000-0002-3531-7388

Shihong Lin: 0000-0001-9832-9127

Notes

The authors declare the following competing financial interest(s): A patent application has been filed based on the work reported in the manuscript.

ACKNOWLEDGMENTS

L.S. is thankful to the support from China Scholarship Council. S.L. acknowledges the support from National Science Foundation via Grant CBET 1739884. G.K.J. acknowledges the Department of Energy's Nuclear Energy University Program (17-12690).

REFERENCES

(1) Abuhabib, A. A.; Mohammad, A. W.; Hilal, N.; Rahman, R. A.; Shafie, A. H. Nanofiltration Membrane Modification by UV Grafting for Salt Rejection and Fouling Resistance Improvement for Brackish Water Desalination. *Desalination* **2012**, *295*, 16−25.

(2) Nanda, D.; Tung, K.-L.; Hsiung, C.-C.; Chuang, C.-J.; Ruaan, R.-C.; Chiang, Y.-C.; Chen, C.-S.; Wu, T.-H. Effect of Solution Chemistry on Water Softening Using Charged Nanofiltration Membranes. *Desalination* **2008**, *234*, 344−353.

(3) Zhu, J.; Tian, M.; Zhang, Y.; Zhang, H.; Liu, J. Fabrication of A Novel "Loose" Nanofiltration Membrane by Facile Blending with Chitosan-Montmorillonite Nanosheets for Dyes Purification. *Chem. Eng. J.* **2015**, *265*, 184−193.

(4) Lin, J.; Ye, W.; Zeng, H.; Yang, H.; Shen, J.; Darvishmanesh, S.; Luis, P.; Sotto, A.; Van Der Bruggen, B. Fractionation of Direct Dyes and Salts in Aqueous Solution Using Loose Nanofiltration Membranes. *J. Membr. Sci.* **2015**, *477*, 183−193.

(5) Zhu, J.; Tian, M.; Hou, J.; Wang, J.; Lin, J.; Zhang, Y.; Liu, J.; Van Der Bruggen, B. Surface Zwitterionic Functionalized Graphene Oxide for a Novel Loose Nanofiltration Membrane. *J. Mater. Chem. A* **2016**, *4*, 1980−1990.

(6) Shan, L.; Gu, J.; Fan, H.; Ji, S.; Zhang, G. Microphase Diffusion-Controlled Interfacial Polymerization for an Ultrahigh Permeability Nanofiltration Membrane. *ACS Appl. Mater. Interfaces* **2017**, *9*, 44820−44827.

(7) Nghiem, L. D.; Schäfer, A. I.; Elimelech, M. Pharmaceutical Retention Mechanisms by Nanofiltration Membranes. *Environ. Sci. Technol.* **2005**, *39*, 7698−7705.

(8) Nghiem, L. D.; Schäfer, A. I.; Elimelech, M. Removal of Natural Hormones by Nanofiltration Membranes: Measurement, Modeling, and Mechanisms. *Environ. Sci. Technol.* **2004**, *38*, 1888−1896.

(9) Van Der Bruggen, B.; Everaert, K.; Wilms, D.; Vandecasteele, C. Application of Nanofiltration for Removal ff Pesticides, Nitrate and Hardness From Ground Water: Rejection Properties And Economic Evaluation. *J. Membr. Sci.* **2001**, *193*, 239−248.

(10) Wang, L.; Ji, S.; Wang, N.; Zhang, R.; Zhang, G.; Li, J.-R. One-Step Self-Assembly Fabrication of Amphiphilic Hyperbranched Polymer Composite Membrane From Aqueous Emulsion For Dye Desalination. *J. Membr. Sci.* **2014**, *452*, 143−151.

(11) Krasner, S. W.; Weinberg, H. S.; Richardson, S. D.; Pastor, S. J.; Chinn, R.; Sclimenti, M. J.; Onstad, G. D.; Thruston, A. D. Occurrence of A New Generation Of Disinfection Byproducts. *Environ. Sci. Technol.* **2006**, *40*, 7175−7185.

(12) Wenk, J.; Aeschbacher, M.; Salhi, E.; Canonica, S.; von Gunten, U. V.; Sander, M. Chemical Oxidation of Dissolved Organic Matter by Chlorine Dioxide, Chlorine, And Ozone: Effects On Its Optical And Antioxidant Properties. *Environ. Sci. Technol.* **2013**, *47*, 11147−11156.

(13) Lu, J.; Zhang, T.; Ma, J.; Chen, Z. Evaluation of Disinfection By-Products Formation During Chlorination and Chloramination Of Dissolved Natural Organic Matter Fractions Isolated from A Filtered River Water. *J. Hazard. Mater.* **2009**, *162*, 140−145.

(14) Werber, J. R.; Deshmukh, A.; Elimelech, M. The Critical Need for Increased Selectivity, Not Increased Water Permeability, For Desalination Membranes. *Environ. Sci. Technol. Lett.* **2016**, *3*, 112−120.

(15) Schäfer, A. I.; Fane, A. G.; Waite, T. D. Cost Factors and Chemical Pretreatment Effects In The Membrane Filtration Of Waters Containing Natural Organic Matter. *Water Res.* **2001**, *35* (6), 1509−1517.

(16) Wang, L.; Wang, N.; Zhang, G.; Ji, S. Covalent Crosslinked Assembly of Tubular Ceramic-Based Multilayer Nanofiltration Membranes for Dye Desalination. *AIChE J.* **2013**, *59* (10), 3834−3842.

(17) Zhang, R.; Ji, S.; Wang, N.; Wang, L.; Zhang, G.; Li, J.-R. Coordination-Driven in Situ Self-Assembly Strategy for The Preparation of Metal-Organic Framework Hybrid Membranes. *Angew. Chem.* **2014**, *126*, 9933−9937.

(18) Tieke, B.; Toutianoush, A.; Jin, W. Selective Transport of Ions and Molecules Across Layer-By-Layer Assembled Membranes of Polyelectrolytes, P-Sulfonato-Calix[*N*]Arenes And Prussian Blue-Type Complex Salts. *Adv. Colloid Interface Sci.* **2005**, *116*, 121−131.

(19) Duong, P. H. H.; Zuo, J.; Chung, T.-S. Highly Crosslinked Layer-By-Layer Polyelectrolyte FO Membranes: Understanding Effects of Salt Concentration and Deposition Time On FO Performance. *J. Membr. Sci.* **2013**, *427*, 411−421.

(20) Tang, C. Y.; Kwon, Y.-N.; Leckie, J. O. Effect of Membrane Chemistry and Coating Layer On Physiochemical Properties Of Thin Film Composite Polyamide RO And NF Membranes II. Membrane Physiochemical Properties and Their Dependence on Polyamide And Coating Layers. *Desalination* **2009**, *242*, 168−182.

(21) Qiu, C.; Qi, S.; Tang, C. Y. Synthesis of High Flux Forward Osmosis Membranes by Chemically Crosslinked Layer-By-Layer Polyelectrolytes. *J. Membr. Sci.* **2011**, *381*, 74−80.

(22) Toutianoush, A.; Jin, W.; Deligöz, H.; Tieke, B. Polyelectrolyte Multilayer Membranes for Desalination Of Aqueous Salt Solutions And Seawater Under Reverse Osmosis Conditions. *Appl. Surf. Sci.* **2005**, *246*, 437−443.

(23) Wu, C.; Zhao, L.; Zhang, Y. Ph-Responsive Nanofiltration Membranes Based on Porphyrin Supramolecular Self-Assembly by Layer-By-Layer Technique. *RSC Adv.* **2017**, *7*, 47397−47406.

(24) Qin, Z.; Ren, X.; Shan, L.; Guo, H.; Geng, C.; Zhang, G.; Ji, S.; Liang, Y. Nacrelike-Structured Multilayered Polyelectrolyte/Calcium Carbonate Nanocomposite Membrane Via Ca-Incorporated Layer-By-Layer-Assembly and CO_2-Induced Biomineralization. *J. Membr. Sci.* **2016**, *498*, 180−191.

(25) Shan, W.; Bacchin, P.; Aimar, P.; Bruening, M. L.; Tarabara, V. V. Polyelectrolyte Multilayer Films as Backflushable Nanofiltration Membranes with Tunable Hydrophilicity and Surface Charge. *J. Membr. Sci.* **2010**, *349*, 268−278.

(26) Ahmadiannamini, P.; Bruening, M. L.; Tarabara, V. V. Sacrificial Polyelectrolyte Multilayer Coatings as An Approach to Membrane Fouling Control: Disassembly and Regeneration Mechanisms. *J. Membr. Sci.* **2015**, *491*, 149−158.

(27) Malaisamy, R.; Bruening, M. L. High-Flux Nanofiltration Membranes Prepared by Adsorption of Multilayer Polyelectrolyte Membranes on Polymeric Supports. *Langmuir* **2005**, *21*, 10587−10592.

(28) Ba, C.; Ladner, D. A.; Economy, J. Using Polyelectrolyte Coatings to Improve Fouling Resistance of A Positively Charged Nanofiltration Membrane. *J. Membr. Sci.* **2010**, *347*, 250−259.

(29) Hu, M.; Mi, B. Layer-By-Layer Assembly of Graphene Oxide Membranes via Electrostatic Interaction. *J. Membr. Sci.* **2014**, *469*, 80−87.

DOI: 10.1021/acs.estlett.8b00430
Environ. Sci. Technol. Lett. 2018, 5, 668−674

(30) Cho, K. L.; Hill, A. J.; Caruso, F.; Kentish, S. E. Chlorine Resistant Glutaraldehyde Crosslinked Polyelectrolyte Multilayer Membranes for Desalination. *Adv. Mater.* **2015**, *27*, 2791−2796.
(31) Manne, S.; Gaub, H. E. Molecular-Organization of Surfactants at Solid-Liquid Interfaces. *Science* **1995**, *270*, 1480−1482.
(32) Gragson, D. E.; Mccarty, B. M.; Richmond, G. L. Ordering of Interfacial Water Molecules at The Charged Air/Water Interface Observed by Vibrational Sum Frequency Generation. *J. Am. Chem. Soc.* **1997**, *119*, 6144−6152.
(33) Johnson, C. M.; Tyrode, E. Study of The Adsorption of Sodium Dodecyl Sulfate (SDS) at the Air/Water Interface: Targeting the Sulfate Headgroup Using Vibrational Sum Frequency Spectroscopy. *Phys. Chem. Chem. Phys.* **2005**, *7*, 2635−2640.
(34) Tiberg, F.; Brinck, J.; Grant, L. Adsorption and Surface-Induced Self-Assembly of Surfactants at The Solid-Aqueous Interface. *Curr. Opin. Colloid Interface Sci.* **1999**, *4*, 411−419.
(35) Richard, C.; Balavoine, F.; Schultz, P.; Ebbesen, T. W.; Mioskowski, C. Supramolecular Self-Assembly of Lipid Derivatives on Carbon Nanotubes. *Science* **2003**, *300*, 775−778.
(36) Tummala, N. R.; Striolo, A. Role of Counterion Condensation in The Self-Assembly of SDS Surfactants at The Water-Graphite Interface. *J. Phys. Chem. B* **2008**, *112*, 1987−2000.
(37) Jaschke, M.; Butt, H.-J.; Gaub, H. E.; Manne, S. Surfactant Aggregates at A Metal Surface. *Langmuir* **1997**, *13*, 1381−1384.
(38) Ko, X.; Sharma, S. Adsorption and Self-Assembly of Surfactants on Metal-Water Interfaces. *J. Phys. Chem. B* **2017**, *121*, 10364−10370.
(39) Luokkala, B. B.; Garoff, S.; Suter, R. M. Using X-Ray Reflectivity to Determine the Structure of Surfactant Monolayers. *Phys. Rev. E: Stat. Phys., Plasmas, Fluids, Relat. Interdiscip. Top.* **2000**, *62*, 2405−2415.
(40) Vogel, A. I. *A Text-Book of Practical Organic Chemistry Including Qualitative Organic Analysis*; Longmans Green and Co.: London, 1991; pp 1413−1422.
(41) Prosser, A. J.; Franses, E. I. Infrared Reflection Absorption Spectroscopy (IRRAS) Of Aqueous Nonsurfactant Salts, Ionic Surfactants, And Mixed Ionic Surfactants. *Langmuir* **2002**, *18*, 9234−9242.
(42) Sperline, R. P. Infrared Spectroscopic Study of The Crystalline Phases of Sodium Dodecyl Sulfate. *Langmuir* **1997**, *13*, 3715−3726.
(43) Viana, R. B.; da Silva, A. B. F. D.; Pimentel, A. S. Infrared Spectroscopy of Anionic, Cationic, And Zwitterionic Surfactants. *Adv. Phys. Chem.* **2012**, *2012*, 1−14.
(44) Shan, L.; Guo, H.; Qin, Z.; Wang, N.; Ji, S.; Zhang, G.; Zhang, Z. Covalent Crosslinked Polyelectrolyte Complex Membrane with High Negative Charges Towards Anti-Natural Organic Matter Fouling Nanofiltration. *RSC Adv.* **2015**, *5*, 11515−11523.
(45) Yuan, W.; Zydney, A. L. Humic Acid Fouling During Ultrafiltration. *Environ. Sci. Technol.* **2000**, *34*, 5043−5050.
(46) Katsoufidou, K.; Yiantsios, S. G.; Karabelas, A. J. A Study of Ultrafiltration Membrane Fouling by Humic Acids And Flux Recovery By Backwashing: Experiments And Modeling. *J. Membr. Sci.* **2005**, *266*, 40−50.
(47) Lin, T.; Lu, Z.; Chen, W. Interaction Mechanisms of Humic Acid Combined with Calcium Ions On Membrane Fouling At Different Conditions In An Ultrafiltration System. *Desalination* **2015**, *357*, 26−35.
(48) Wang, Z.; Ding, J.; Xie, P.; Chen, Y.; Wan, Y.; Wang, S. Formation of Halogenated By-Products During Chemical Cleaning of Humic Acid-Fouled UF Membrane by Sodium Hypochlorite Solution. *Chem. Eng. J.* **2018**, *332*, 76−84.
(49) Xie, M.; Nghiem, L. D.; Price, W. E.; Elimelech, M. Impact of Humic Acid Fouling on Membrane Performance and Transport of Pharmaceutically Active Compounds In Forward Osmosis. *Water Res.* **2013**, *47*, 4567−4575.
(50) Ates, N.; Yilmaz, L.; Kitis, M.; Yetis, U. Removal of Disinfection By-Product Precursors by UF And NF Membranes in Low-SUVA Waters. *J. Membr. Sci.* **2009**, *328*, 104−112.
(51) Peeva, P. D.; Palupi, A. E.; Ulbricht, M. Ultrafiltration of Humic Acid Solutions Through Unmodified and Surface Functionalized Low-Fouling Polyethersulfone Membranes - Effects of Feed Properties, Molecular Weight Cut-Off and Membrane Chemistry on Fouling Behavior and Cleanability. *Sep. Purif. Technol.* **2011**, *81*, 124−133.
(52) Zhao, Y.; Li, N.; Xia, S. Polyamide Nanofiltration Membranes Modified with Zn-Al Layered Double Hydroxides for Natural Organic Matter Removal. *Compos. Sci. Technol.* **2016**, *132*, 84−92.
(53) Adams, F. V.; Nxumalo, E. N.; Krause, R. W. M.; Hoek, E. M. V.; Mamba, B. B. Application of Polysulfone/Cyclodextrin Mixed-Matrix Membranes in the Removal of Natural Organic Matter from Water. *Phys. Chem. Earth* **2014**, *67−69*, 71−78.
(54) Shan, L.; Fan, H.; Guo, H.; Ji, S.; Zhang, G. Natural Organic Matter Fouling Behaviors on Superwetting Nanofiltration Membranes. *Water Res.* **2016**, *93*, 121−132.
(55) Xia, S.; Yao, L.; Zhao, Y.; Li, N.; Zheng, Y. Preparation of Graphene Oxide Modified Polyamide Thin Film Composite Membranes with Improved Hydrophilicity for Natural Organic Matter Removal. *Chem. Eng. J.* **2015**, *280*, 720−727.
(56) Xia, S.; Ni, M. Preparation of Poly(Vinylidene Fluoride) Membranes with Graphene Oxide Addition for Natural Organic Matter Removal. *J. Membr. Sci.* **2015**, *473*, 54−62.
(57) Kumar, M.; Gholamvand, Z.; Morrissey, A.; Nolan, K.; Ulbricht, M.; Lawler, J. Preparation and Characterization of Low Fouling Novel Hybrid Ultrafiltration Membranes Based on The Blends of GO-Tio_2 Nanocomposite and Polysulfone for Humic Acid Removal. *J. Membr. Sci.* **2016**, *506*, 38−49.
(58) Alsohaimi, I. H.; Kumar, M.; Algamdi, M. S.; Khan, M. A.; Nolan, K.; Lawler, J. Antifouling Hybrid Ultrafiltration Membranes with High Selectivity Fabricated From Polysulfone And Sulfonic Acid Functionalized Tio_2 Nanotubes. *Chem. Eng. J.* **2017**, *316*, 573−583.
(59) Huang, Y.; Sun, J.; Wu, D.; Feng, X. Layer-By-Layer Self-Assembled Chitosan/PAA Nanofiltration Membranes. *Sep. Purif. Technol.* **2018**, *207*, 142−150.
(60) Luo, J.; Wan, Y. Effects of pH And Salt on Nanofiltration-a Critical Review. *J. Membr. Sci.* **2013**, *438*, 18−28.

DOI: 10.1021/acs.estlett.8b00430
Environ. Sci. Technol. Lett. 2018, 5, 668−674